ADVANCED BIOLOGY
www.advanced-bio.com

Photobiologically Directed Assembly of Gold Nanoparticles

Julia Dietler, Chen Liang, Saskia Frank, Ann-Kathrin Müller, Andreas Greiner, and Andreas Möglich**

In nature, photoreceptor proteins undergo molecular responses to light, that exhibit supreme fidelity in time and space and generally occur under mild reaction conditions. To unlock these traits for material science, the light-induced homodimerization of light-oxygen-voltage (LOV) photoreceptors is leveraged to control the assembly of gold nanoparticles. Conjugated to genetically encodable LOV proteins, the nanoparticles are monodispersed in darkness but rapidly assemble into large aggregates upon blue-light exposure. The work establishes a new modality for reaction control in macromolecular chemistry and thus augurs enhanced precision in space and time in diverse applications of gold nanoparticles.

Adaptations to light abound in biology across wide time and length scales. At the molecular level, these adaptations rely on sensory photoreceptor proteins that absorb photons and initiate photochemical and biochemical reaction cascades with exquisite resolution in time and space. Often, these reactions entail the formation or dissolution of non-covalent interactions among proteins and other biomolecules. Notably, photoreceptors are genetically encoded and generally operate in aqueous milieu under mild reaction conditions. These core aspects are exemplified by the light-oxygen-voltage (LOV) photoreceptor class which respond to blue light via flavin nucleotide chromophores (**Figure 1**A).[1] Certain LOV receptors undergo light-controlled homo- or heterodimerization reactions (Figure 1B), which have been harnessed to optogenetically control a cohort of cellular processes.[2]

Here, we extend the concept of photobiological reaction control from biology to materials science. We develop the on-demand assembly of gold nanoparticles (AuNPs) as model nanoparticles via photobiological direction by associating LOV receptors (Figure 1C). Nanoparticles in general are of fundamental interest for a variety of industrial processes.[3,4] AuNPs in specific underpin diverse applications in, e.g., biological sensing and imaging,[5–7] drug delivery,[8] and intracellular gene regulation.[9] Moreover, AuNPs of various shapes and sizes were ordered and arranged in defined architectures.[5–12] Nanoparticle assembly was for instance controlled by various ligands,[13–15] but also by external stimuli, such as magnetic fields or light.[16–24] These advances notwithstanding, the controlled higher-order assembly in response to external cues remains challenging, but worthwhile to explore because it could significantly extend the application scope of AuNPs. In particular, the interfacing of the inorganic nanoparticles with genetically encodable, adaptable, light-responsive proteins augurs innovative use cases. As a cue signal, light appears ideal as it can be applied non-invasively and supports high spatial and temporal precision, which is not least evidenced by ample applications in biology and biotechnology.[2]

To achieve LOV-directed AuNP assembly, we envisioned a direct link between the organic photoreceptor proteins and the inorganic particles. Initial attempts to covalently couple the light-responsive proteins to citrate-capped AuNPs via gold sulfide bonds failed, because unspecific interactions (owing to cysteine residues within the protein and to the presence of salt ions, required for protein stability) invariably triggered nanoparticle aggregation and precipitation.[25,26] Therefore, we opted for the non-covalent attachment of the LOV receptors through nickel coordination chemistry. This strategy necessitates that the photoreceptors be equipped with hexa-histidine (His_6) tags and the AuNPs be functionalized with Ni^{2+}-nitrilotriacetic acid (NTA) ligands (Figure 1C).[10,21,27] We selected two well-characterized LOV domains from *Phaeodactylum tricornutum* aureochrome 1a (*Pt*aur) and from *Neurospora crassa* Vivid (*Nc*VVD), both previously shown to undergo light-induced homodimerization[28,29] and used to bestow light sensitivity on cellular processes.[2] Size-exclusion chromatography (SEC) confirmed that in their unmodified forms both LOV proteins adopt homogenous states in either darkness or blue light (Figure S1, Supporting Information); the apparent molecular size under blue light was higher, indicative of light-induced dimerization. Next, we introduced His_6 tags at either the N or C termini of the LOV domains, separated by short glycine-serine linkers. N-terminal modification of *Pt*aur led to constitutive dimerization independent of light and accompanied by aggregation, whereas C-terminal modification incurred protein insolubility. The sensitivity of the *Pt*aur N- and C-terminal segments likely

J. Dietler, S. Frank, Prof. A. Möglich
Department of Biochemistry, Photobiochemistry
University of Bayreuth
Bayreuth D-95440, Germany
E-mail: andreas.moeglich@uni-bayreuth.de
C. Liang, A.-K. Müller, Prof. A. Greiner
Macromolecular Chemistry and Bavarian Polymer Institute
University of Bayreuth
Bayreuth D-95440, Germany
E-mail: andreas.greiner@uni-bayreuth.de
The ORCID identification number(s) for the author(s) of this article can be found under https://doi.org/10.1002/adbi.202000179.

DOI: 10.1002/adbi.202000179

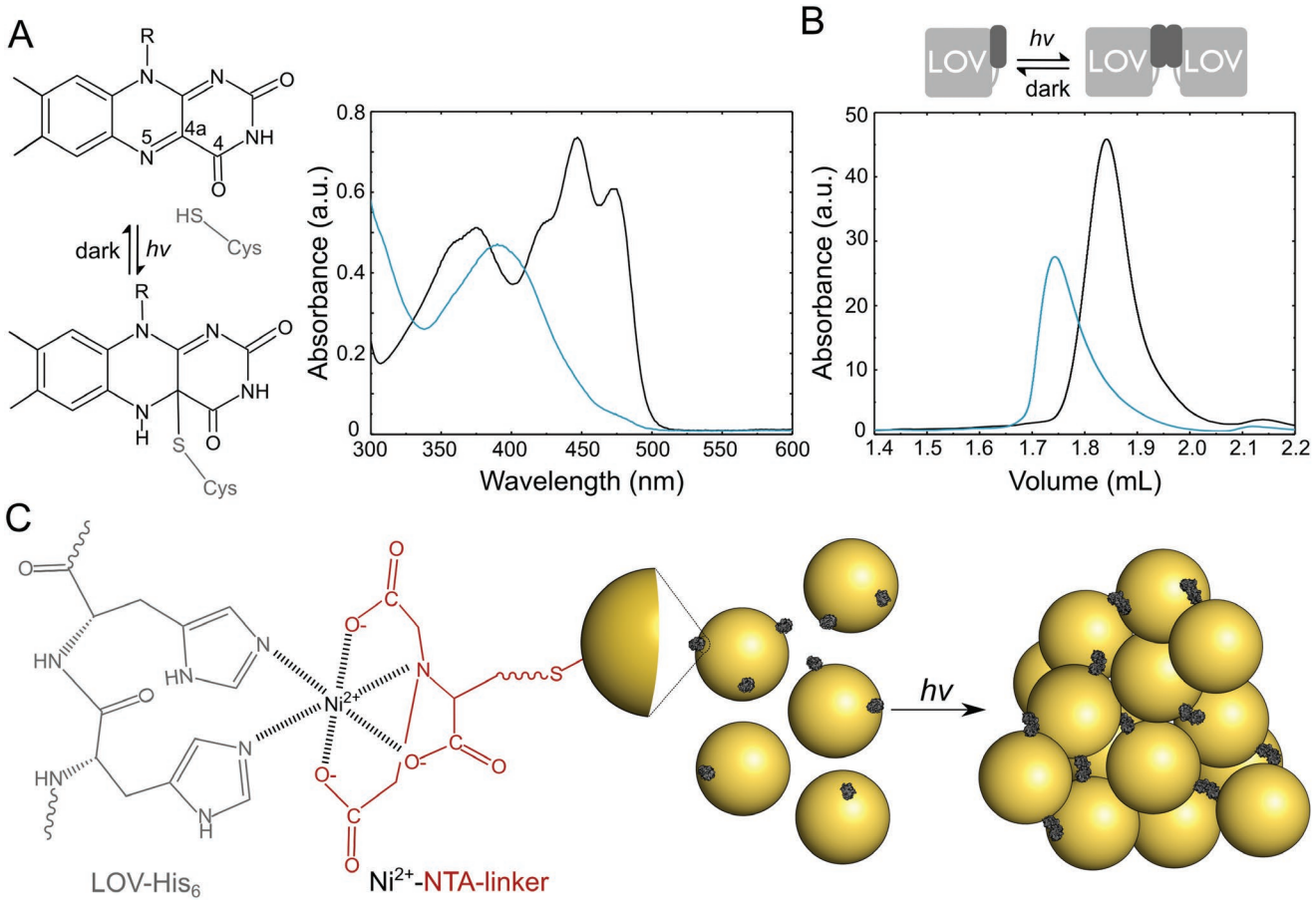

Figure 1. Photobiologically directed assembly of gold nanoparticles (AuNPs) by light-oxygen-voltage (LOV) photoreceptors. A) Simplified LOV photocycle, showing the oxidized quinone state of flavin nucleotide non-covalently bound within the LOV domain in the dark, and the light-induced formation of a covalent thioadduct between a conserved cysteine residue (Cys) and the C4a atom of the flavin molecule. The adduct form spontaneously recovers to restore the dark-adapted state. The photocycle can be observed spectroscopically by absorption of the dark-adapted (black) and light-adapted states (blue). B) Size-exclusion chromatography of *Nc*VVD-His_6 in darkness (black traces) and following blue-light exposure (blue traces). C) To achieve light-induced AuNP assembly, associating LOV domains are immobilized on the particle surface by Ni^{2+}-NTA coordination chemistry. Exposure to blue light triggers the dimerization of the LOV domain, which consequently drives the assembly of AuNPs.

owes to them contributing to the light-driven homodimerization.[30,31] Similarly, introduction of the His_6 tag at the N terminus of *Nc*VVD caused protein insolubility, consistent with the crucial role of this protein segment in dimerization.[32] By contrast, appendage to the C terminus (*Nc*VVD-His_6) was tolerated, and light-induced dimerization of *Nc*VVD was preserved as assessed by SEC (Figure 1B).

To allow conjugation of the *Nc*VVD-His_6 protein to the particles, we synthesized citrate-capped AuNPs according to Frens[33,34] and subsequently equipped their surface with Ni^{2+}-NTA groups via ligand exchange and Ni^{2+} complexation (Figure S2, Supporting Information). Owing to the sensitivity of the surface plasmon resonance (SPR) signal to surface properties,[35] the functionalization with the Ni^{2+}-NTA groups induced a shift of the SPR absorption band of the AuNPs, that could be followed spectroscopically (Figure S3, Supporting Information). Transmission electron microscopy (TEM) revealed that prior to and after Ni^{2+}-NTA functionalization, the AuNPs did not associate and were essentially monodisperse with a mean diameter of (17.7 ± 1.6) nm (Figure S4, Supporting Information). Dynamic light scattering (DLS) showed similar average sizes of (21.8 ± 3.6) and (30.6 ± 3.4) nm for the citrate-capped and the Ni^{2+}-NTA-ligated AuNPs, respectively (Figure S5, Supporting Information). Based on the functionalization of AuNPs with similar ligands,[36] we estimate that around 4000 NTA ligands are bound to the surface of each AuNP.

Next, we assessed the interaction of *Nc*VVD-His_6 and the Ni^{2+}-NTA functionalized AuNPs. As light scattering scales with the sixth power of particle dimensions, the DLS signal is dominated by larger particles present in solution. To obtain a more accurate view of particle sizes and distributions, we hence switched to asymmetric flow field-flow fractionation (AF4) (Figures S6 and S7, Supporting Information). While the citrate-capped and the Ni^{2+}-NTA-functionalized AuNPs eluted with apparent radii of (11 ± 2) nm and (12 ± 2) nm, respectively, for the main particle fraction, addition of a fiftyfold molar excess of *Nc*VVD-His_6 induced a shift to (18 ± 2) nm. Given a protein diameter of ≈4 nm, these results indicate the association of LOV proteins to the AuNPs. When exposed to 450-nm light, the

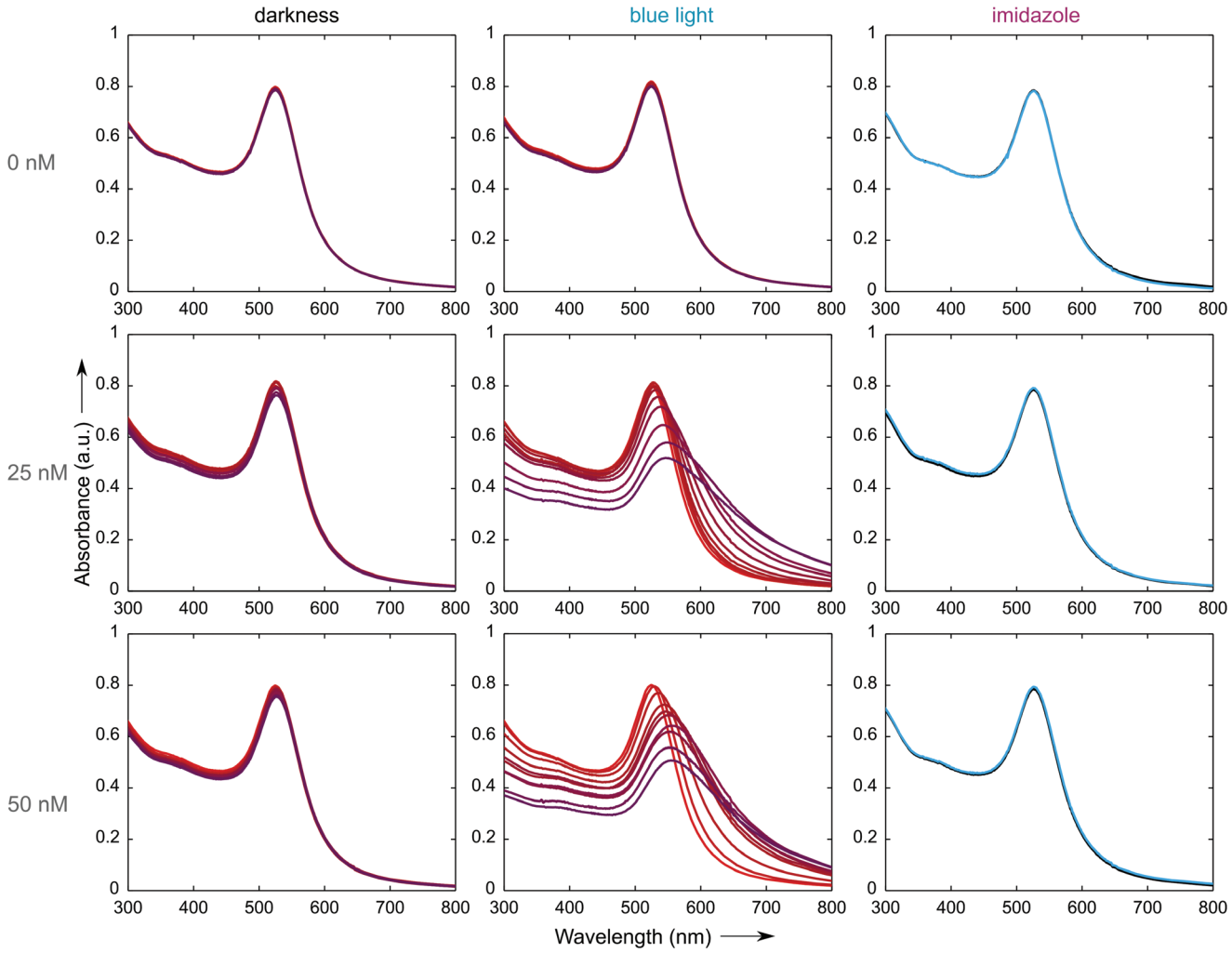

Figure 2. Blue-light exposure drives the assembly of Ni^{2+}-NTA functionalized AuNPs coupled to *Nc*VVD-His_6. Time series of UV–vis spectra of Ni^{2+}-NTA functionalized AuNPs in the absence and presence of 25×10^{-9} or 50×10^{-9} M *Nc*VVD-His_6. Spectra were acquired at 2, 5, 10, 15, 20, 30, 40, 60, and 90 min after protein addition (from top to bottom). Ni^{2+}-NTA functionalized AuNPs show a strong absorption with a maximum at 524 nm independent of illumination. In presence of *Nc*VVD-His_6, blue light induces a broadening of the plasmon peak and a shift toward greater wavelengths, indicating the assembly of AuNPs. The velocity of light-directed assembly can be set by the LOV protein concentration. As control, Ni^{2+}-NTA functionalized AuNPs were incubated in the presence of imidazole without or with different concentrations of *Nc*VVD-His_6 (right panels). After 90 min of incubation in either darkness (black traces) or under constant blue light (blue traces) no significant spectral changes could be detected. Imidazole competes with the His_6 tag for NTA binding and thus prevents light-induced particle assembly.

solution of *Nc*VVD-conjugated AuNPs rapidly changed color from light red to purple, indicative of altered plasmon resonance and nanoparticle assembly. The formation of such blue light-induced particle clusters was qualitatively confirmed by AF4 measurements during which a purple precipitate of high molecular weight formed on the analysis membrane (Figure S7, Supporting Information).

To better characterize the light-induced association reaction, we followed its kinetics by UV-vis absorption spectroscopy (**Figure 2**). In the absence of the LOV protein, the Ni^{2+}-NTA-AuNPs at 0.9×10^{-9} M concentration exhibited broad absorption overlain by a narrower SPR band peaking at 524 nm, irrespective of whether the samples were kept in darkness or illuminated with blue light. Addition of 25×10^{-9} or 50×10^{-9} M *Nc*VVD-His_6 did not induce significant spectral changes provided the samples were kept in the dark. When exposed to 450-nm light, over the course of 90 min, the SPR band successively broadened, and its maximum shifted to longer wavelengths up to 630 nm. The substantial spectral shift of more than 100 nm reflects the formation of heterogeneous, large-scale nanoparticle assemblies. The kinetics of this process were faster for 50×10^{-9} M *Nc*VVD-His_6 than for 25×10^{-9} M. By approximating the shape of the *Nc*VVD-His_6 protein as a sphere of 4 nm diameter, we calculate that at maximum around 30 protein molecules can be accommodated on the surface of each particle. Notably, the *Nc*VVD-His_6 concentrations of 25×10^{-9} and 50×10^{-9} M correspond to molar ratios of 28 and 56 proteins per nanoparticle, respectively. Reduction of the protein amount severely slowed down the assembly process to the extent that at 6.25×10^{-9} M *Nc*VVD-His_6 almost no spectral

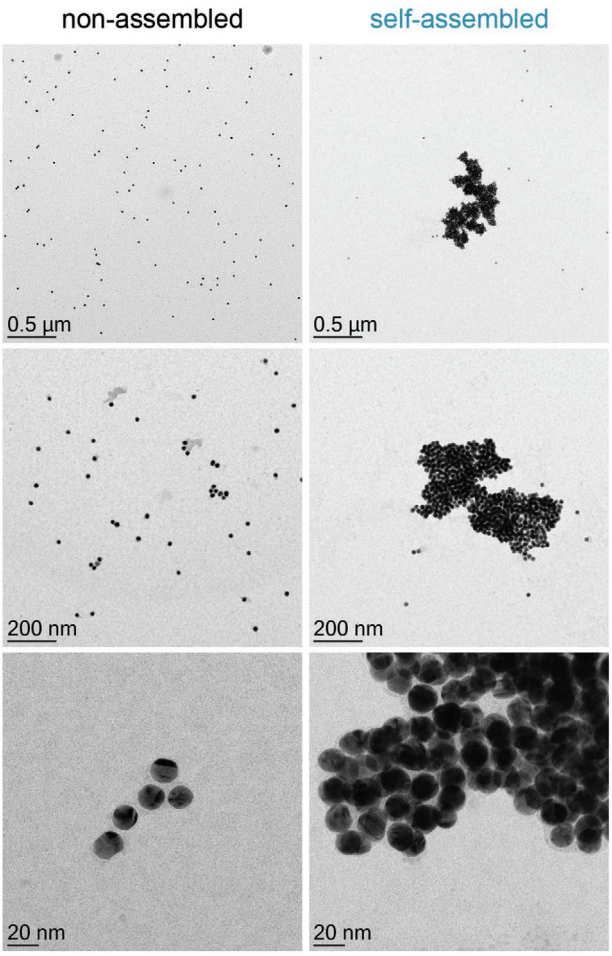

Figure 3. Light-induced assembly of nanoparticles. Transmission electron microscopy images of Ni^{2+}-NTA functionalized AuNPs in the presence of *Nc*VVD-His_6 in darkness (left) or following blue-light exposure (right). In the absence of light, LOV-coupled AuNPs are evenly distributed and do not interact, whereas light-programmed association of the LOV receptors directs the assembly of the particles, culminating in the formation of extended networks with up to micrometer dimensions.

changes could be observed upon illumination (Figure S8, Supporting Information). Addition of imidazole, which competes for binding to the Ni^{2+}-NTA group, abrogated any light-induced spectral changes (Figure 2).

We next analyzed by transmission electron microscopy (TEM) the size distribution of Ni^{2+}-NTA-AuNPs conjugated with *Nc*VVD-His_6 in darkness and under blue light (**Figure 3**). Prior to illumination, the AuNPs appeared monodisperse and evenly distributed on the TEM grid, with a minor population of particles in smaller groups but without forming immediate contact. By contrast, after exposure to blue light, most particles were in direct contact and formed stacked, amorphous assemblies of up to 1.5 µm in size. Notably, the assemblies formed irreversibly as neither prolonged incubation in darkness nor the addition of imidazole could dissolve them. We ascribe this observation to fusion of the nanoparticles once they have been brought into spatial proximity.[26] The AuNPs thus resisted attempts at dispersion.

Our results showcase AuNP assembly at will through photobiological direction by LOV receptors. By wedding inorganic and proteinaceous building blocks, we synthesize a composite system with emergent properties and thereby establish a new paradigm for reaction control in macromolecular chemistry. We thus lay the foundation for future applications at the interface of colloidal chemistry and biochemistry, as the principal strategy generally extends to diverse nanoparticles of various shape, composition and properties. The use of light triggers stands to permit the controlled nanoparticle assembly with superior spatial resolution, for example by lithography. Although not exploited here, we note that owing to genetic encoding and thereby identity, sensory photoreceptors can be readily attached to other proteins and biomolecules, or displayed on the surface of cells.[37] Doing so enables the defined incorporation of nanoparticles into complex biological circuits and reaction cascades. Of advantage, biological systems are generally malleable and can be adapted in their properties to meet specific application demands. As a case in point, the lifetime of the light-adapted state of LOV receptors, and therefore their effective light sensitivity at photostationary state, can be routinely varied across several orders of magnitude.[38,39] The combination of suitably modified, light-sensitive biological systems with nanoparticles thus augurs novel applications in biology and materials science alike. For instance, the light-triggered assembly of AuNPs, presently configured to be irreversible, may be harnessed for security purposes, such as monitoring the light exposure of sensitive materials.

Experimental Section

Expression and Purification of LOV Proteins: The genes of the N-terminally truncated short-LOV protein *Neurospora crassa* Vivid (NcVVD) (residues 37–186, including the mutations C71V and N56K)[29,32] and the A′α-LOV-Jα module of *Phaeodactylum tricornutum* Aureo1a (*Pt*aur) (residues 235–378) were obtained by gene synthesis (GeneArt, Regensburg, Germany) and cloned by Gibson assembly[40] into expression vectors. For the preparation of untagged protein and variants with N- or C-terminal His_6 tags, the vectors pET-19b-SUMO, pET-28c, and pET-41a were used, respectively. Where applicable, a $(GS)_5$-linker was inserted between the LOV core protein and the His_6 tags.

For expression, the plasmid constructs were transformed into *Escherichia coli* BL21(DE3) CmpX13 cells.[41] 800 mL of lysogeny broth (LB) medium, supplemented with 50 µg mL^{-1} kanamycin, were inoculated with single clones and incubated at 37 °C and 200 rpm until an optical density at 600 nm of 0.6–0.8 was reached. At this point, expression was induced with 1×10^{-3} M isopropyl β-D-1-thiogalactopyranoside (IPTG), the temperature was lowered to 16 °C, and the incubation continued for ≈18 h under constant blue-light illumination (450 nm, 100 µW cm^{-2}). The light intensity was determined with a power meter (model 842-PE, Newport) and a silicon photodetector (model 918D-UV-OD3, Newport). Cells were harvested by centrifugation and lysed by ultrasound. The cell lysate was cleared by centrifugation and purified by Ni:NTA affinity chromatography under exclusion of blue light. Fractions eluted by imidazole from the affinity column were analyzed by denaturing polyacrylamide gel electrophoresis (PAGE) and pooled. Proteins with terminal His_6 tags expressed from the pET-28c and pET-41a vectors were directly dialyzed into storage buffer (50×10^{-3} M Tris, 300×10^{-3} M NaCl, 50% (w/v) glycerol, pH 8). In case of the SUMO-tagged LOV domains, the N-terminal His_6-SUMO tags were removed by Senp2 cleavage, followed by a reverse Ni:NTA affinity chromatography. The resulting, untagged LOV protein was dialyzed into storage buffer as above. At all times during purification, proteins were handled under dim red light, and

*Nc*VVD constructs were kept in buffers containing 10% (w/v) glycerol to aid stability. Protein purity was assessed by denaturing PAGE analyses, and protein concentration was determined by UV–vis spectroscopy using an absorption coefficient of the flavin mononucleotide cofactor at 450 nm of 12 500 M^{-1} cm^{-1}.

Synthesis of AuNPs: Gold chloride trihydrate (>99%), nickel (II) chloride (anhydrous, 98%), and *N*,*N*′-dicyclohexylcarbodiimide (DCC, 99%) were purchased from Alfa Aesar. Trisodium salt dihydrate (99%) and hydrazine acetate (97%) were bought from Acros Organics. 11-mercaptoundecanoic acid, N_ω,N_α-bis(carboxymethyl)-L-lysine, 1,2-dimethoxyethane (DME, 99%), *N*-hydroxysuccinimide (98%), and zinc (pure, powder) were purchased from Sigma-Aldrich. Acetyl chloride (≥98%) was purchased from Merck. Sodium hydrogen carbonate, chloroform, and dimethylformamide (DMF) were purchased from Fisher Chemical. Sodium sulphate, tris(hydroxymethyl)-aminomethan (Tris), sodium chloride, glycerol and imidazole were purchased from Carl Roth. Hydrochloric acid (37%) and acetic acid were purchased from VWR. Milli-Q water was used throughout the experiments. To avoid unwanted nucleation during the synthesis and aggregation of gold colloid solutions, all glassware and magnetic stir bars used in the syntheses were thoroughly cleaned in aqua regia (HCl/HNO_3 3:1), rinsed in distilled water and then dried prior to use.

400 mL of an aqueous solution of $HAuCl_4$ (2.5×10^{-4} M) was heated to boiling, ensued by the addition of 10.4 mL trisodium citrate solution [1% (w/w)] under continuous stirring. Within 5 min of boiling, the solution gradually changed color from yellow to white, grey, faint blue, violet, and finally red, indicating the formation of AuNPs. The reaction mixture was boiled for another 30 min and then cooled down to ambient temperature during mild stirring. The solution of AuNPs was stable and stored at 4 °C.

Synthesis of Thiolated Nitrilotriacetic Acid (NTA) Ligand: The thiolated NTA group was synthesized by adapting a previously reported procedure (Figure S2, Supporting Information).[10,21,27]

Synthesis of Thiolated Nitrilotriacetic Acid (NTA) Ligand—Synthesis of 11-(acetylthio)undecanoic Acid: A solution of 11-mercaptoundecanoic acid (838 mg, 3.84 mmol) in 67 mL chloroform and 14 mL acetic acid was stirred for 15 min after zinc powder (2.2 g) was added. Then, the solution was cooled to 0 °C, subsequently treated with acetyl chloride (5.33 mL) and stirred overnight. Afterward, zinc was removed by filtration using a pad of Celite, and the filtrate was washed twice with 0.1 M HCl (30 mL) and water (30 mL). The organic deposit was dried above Na_2SO_4, filtered, and concentrated in vacuo. The residue was purified by column chromatography to give compound **1** 650 mg (65%) as a white powder [^{1}H NMR (300 MHz, $CDCl_3$) δ 2.85 (t, 2H), 2.37–2.31 (m, 5H), 1.67–1.48 (m, 4H), 1.37–1.20 (m, 12H)]

Synthesis of Thiolated Nitrilotriacetic Acid (NTA) Ligand—Synthesis of N-[N_ω,N_α-bis(carboxymethyl)-L-lysine] 11-(acetylthio)dodecanamide: A solution of 11-(acetylthio)undecanoic acid (**1**, 164 mg, 0.63 mmol) and *N*-hydroxysuccinimide (NHS, 72.5 mg, 0.63 mmol) in 9 mL anhydrous 1,2-dimethoxyethane (DME) was cooled to 0 °C, and subsequently *N*,*N*′-dicyclohexylcarbodiimide (157 mg, 0.76 mmol) was added. The solution was kept at 0 °C for 24 h, and afterward the white dicyclohexylurea precipitate was removed by filtration and rinsed with dry DME. The filtrate was concentrated in vacuo, and the resulting white powder NHS ester was used without further purification. The NHS ester was resuspended in acetone (0.63 mL) and ethanol (6.18 mL) and subsequently treated with a solution of N_ω,N_α-bis(carboxymethyl)-L-lysine (164.92 mg, 0.63 mmol) and $NaHCO_3$ (211.68 mg, 2.52 mmol) in water (3.15 mL) at room temperature and stirred for 43 h under argon. Then, the ethanol was removed under reduced pressure and the residue was diluted with water (3.15 mL) and aqueous $NaHCO_3$ solution (0.25 M, 1.26 mL). The resulting white precipitate was filtered and discarded. After acidification of the filtrate with 1.0 M HCl to pH 3, the resulting colloidal suspension was centrifuged (4000 rpm, 25 °C, 20 min), leading to the production of crude product **3**. The pellet was washed with water by repeating the resuspension/centrifugation twice. The resulting residue was lyophilized to give 156 mg (49%) of compound **3** as a pale white solid. [^{1}H NMR (300 MHz, DMSO-d_6) δ 3.45 (d, 4H), 3.31 (t, J = 7.3 Hz, 2H), 2.98 (br, 2H), 2.81 (t, J = 7.2 Hz, 2H), 2.31 (s, 3H), 2.01 (t, J = 7.4 Hz, 2H), 1.64–1.11 (m, 22H).]

Synthesis of Thiolated Nitrilotriacetic Acid (NTA) Ligand—Synthesis of N-[N_ω,N_α-bis(Carboxymethyl)-L-lysine] 11-Mercaptododecanamide (NTA): Hydrazine acetate (147 mg, 1.59 mmol) was added to a solution of *N*-[N_ω,N_α-bis(carboxymethyl)-L-lysine] 11-(acetylthio)dodecanamide (compound **3**, 53 mg, 0.105 mmol) in dimethylformaide (6.5 mL) and afterward bubbled with argon for 20 min at room temperature. The solution was then degassed and again stirred for 20 h under argon. The solvent was removed under reduced pressure, followed by the treatment with 0.05 N HCl (20 mL). The resulting colloidal suspension was centrifuged (4000 rpm, 25 °C, 20 min) to give crude product **4**, denoted NTA hereafter. The supernatant was removed, and the residue was then washed with water by repeating resuspension / centrifugation twice. The product was lyophilized to give 36 mg (74%) of compound **4** as a pale white solid. [^{1}H NMR (300 MHz, DMSO-d_6) δ 3.47 (d, 4H), 3.31 (t, J = 7.3 Hz, 1H), 2.98 (br, 2H), 2.44 (t, J = 7.2 Hz, 2H), 2.01 (t, J = 7.4 Hz, 2H), 1.66–1.10(m, 22H). ^{13}C NMR (75 MHz, DMSO-d_6) δ 174.03, 173.30, 171.92, 64.34, 53.43, 38.26, 35.46, 33.46, 29.37, 28.94, 28.81, 28.54, 27.80, 25.36, 23.81, 23.15] Mass spectrometry: calculated $(M + 1)^+ = 463.247$, observed $(M + 1)^+ = 463.2469$

Synthesis of Thiolated Nitrilotriacetic Acid (NTA) Ligand—Preparation of Ni^{2+}-NTA Functionalized AuNPs in Buffer via Ligand Exchange: 1 mg NTA (**4**) was dissolved in 3 mL of 50×10^{-3} M Tris, 300×10^{-3} M NaCl, 10% (w/v) glycerol, pH 8.0. Next, 5 mL of gold nanoparticle solution was added to the solution, and the mixture was stirred at room temperature overnight. The mixture was then centrifuged at 6000 rpm for 20 min, the supernatant was removed, and the precipitated AuNPs were re-dispersed in the same buffer. 3.5 µL $NiCl_2$ (12.5 mg/20 mL) was added to the AuNP solution, followed by incubation at ambient temperature for 20 min. The solution of Ni^{2+}-NTA-AuNPs was centrifuged at 6000 rpm for 20 min again. The final supernatant was removed, and the Ni^{2+}-NTA-AuNPs were resuspended in 50×10^{-3} M Tris, 300×10^{-3} M NaCl, 10% (w/v) glycerol, pH 8.0. The particles were kept at 4 °C until further use.

The molar concentration of gold atoms, c_{Au}, was determined by inductively coupled plasma optical emission spectrometry, see below. To calculate the concentration of AuNPs, a spherical shape and a uniform face-centered cubic lattice (fcc) structure of the synthesized AuNPs was assumed. The average number of gold atoms per nanoparticle (N) was calculated by Equation (1), where ρ denotes the density for fcc gold (19.3 g cm^{-3}), M is the atomic weight of gold (197 g mol^{-1}), and d is the diameter of the AuNPs (17.7 nm, as measured by TEM)[42]

$$N = \pi/6 \times (\rho d^3/M) \quad (1)$$

The molar concentration of the AuNPs, c_{NP}, was then calculated according to Equation (2)

$$c_{NP} = c_{Au}/N \quad (2)$$

Analytical Methods—Size-Exclusion Chromatography: Size-exclusion chromatography was performed on an ÄKTA pure system and a Superdex 200 Increase 3.2/300 analytical column at 4 °C. The column was equilibrated with buffer containing 50×10^{-3} M Tris/HCl, 100×10^{-3} M NaCl and 5×10^{-3} M β-mercaptoethanol at pH 8.0, and operated at a flow rate of 0.05 mL min^{-1}. Samples were centrifuged at 13 200 × *g* and injected in 30 µL aliquots at a concentration of 50×10^{-6} M. Light-adapted samples were generated by irradiation with blue light (450 nm, 30 mW cm^{-2}, 2 min) immediately prior to injection. The run of the light-adapted sample was performed under constant blue light, while the run of the dark-state sample was conducted under exclusion of light. The elution of the samples was followed by absorption measurements at 280 nm.

Analytical Methods—Transmission Electron Microscopy (TEM): TEM micrographs were obtained on a ZEISS EM922 Omega microscope at an acceleration voltage of 200 keV. Functionalized AuNPs (0.9×10^{-9} M) were incubated with 50×10^{-9} M *Nc*VVD-His_6 either in the absence or presence of blue light irradiation (450 nm, 30 mW cm^{-2}) for 10 min at 4 °C. Then, individual samples were prepared by dripping the protein-AuNPs solution on a carbon-covered copper grid and drying at room temperature overnight. The

images were evaluated with ImageJ. For each sample at least 100 AuNPs were counted.

Analytical Methods—Asymmetric Flow Field-Flow Fractionation (AF4): AF4 measurements were carried out using an AF2000 system with a Smart Stream Splitter from Postnova Analytics (Landsberg am Lech, Germany). The channel had a length and width of 295 and 30 mm, respectively, and was equipped with a spacer height of 350 µm. The separation was conducted on a NovaRC 10 kDa regenerated cellulose membrane. Detection was performed with a UV detector at a wavelength of 270 nm. In addition, the samples were analyzed inline by a multiple angle light scattering (MALS) detector (Postnova Analytics), with 21 observation angles and operated with linearly polarized laser light at 532 nm. Individual runs were conducted as stated in Table S1 in the Supporting Information using 50×10^{-3} M Tris/HCl, 300×10^{-3} M NaCl and 10% (w/v) glycerol at pH 8.0 as eluent. The temperature was kept at 8 °C during the measurement, and the samples were prepared as described in the TEM section. The run of the light-adapted samples was performed under constant illumination, whereas the run of the dark-adapted sample was conducted under exclusion of light. Data from the MALS detector were processed using the Postnova AF2000 control software. A spherical model was used for obtaining the radius of gyration based on the angular dependence of scattered light recorded by the MALS detector.

Analytical Methods—Inductively Coupled Plasma Optical Emission Spectrometry: Measurements were performed on an Avio 200 instrument (Perkin Elmer) in radial viewed plasma with purged polychromator configurations. The measurement was calibrated with four standard solutions at concentrations of 0.1, 0.5, 1, and 10 mg L^{-1}.

Analytical Methods—Nuclear Magnetic Resonance (NMR) Spectroscopy: ^{1}H NMR and ^{13}C NMR spectroscopy was carried out on a Bruker Ultrashield 300 using deuterated chloroform and DMSO as solvents at 300 MHz. Spectra were calibrated by the signal of the residual protons of the deuterated solvents. Spectra were evaluated with the MestReNova software.

Analytical Methods—Mass Spectrometry (MS): Mass spectrometry was performed using direct infusion from an Ultimate 3000 UPLC system (Dionex, Sunnyvale, CA, USA) to a Hybrid Quadrupole Orbitrap system with electrospray ionization (ESI, Thermo Fisher Scientific, Waltham, MA, USA). For the MS analysis, ESI was operated in positive mode. Full scan was applied with a mass range of 80–1200 amu.

Analytical Methods—UV–vis (UV–vis) Absorption Spectroscopy: UV–vis absorption spectroscopy was carried out on an Agilent 8453 UV–vis spectroscopy system together with an Agilent 89090A temperature control accessory. Absorption spectra were recorded in 50×10^{-3} M Tris/HCl, 300×10^{-3} M NaCl, 10% (w/v) glycerol, pH 8.0 right after addition of 0×10^{-9}, 6.25×10^{-9}, 12.5×10^{-9}, 25×10^{-9}, or 50×10^{-9} M of *Nc*VVD-His_6 to 0.9×10^{-9} M of Ni^{2+}-NTA functionalized AuNPs. For kinetic measurements, light-adapted samples were constantly illuminated with 450-nm light (30 mW cm^{-2}), while dark-state samples were kept in darkness. Absorption spectra were recorded before addition of protein and after 2, 5, 10, 15, 20, 30, 40, 60, and 90 min of incubation at 4 °C in low-binding reaction tubes (Eppendorf, DNA LoBind). As a control, the AuNPs were incubated in the presence of 560×10^{-3} M imidazole and 0×10^{-9}, 6.25×10^{-9}, 12.5×10^{-9}, 25×10^{-9}, or 50×10^{-9} M *Nc*VVD-His_6; the analysis was carried out as described above.

Supporting Information

Supporting Information is available from the Wiley Online Library or from the author.

Acknowledgements

Financial support was provided by University of Bayreuth and the Deutsche Forschungsgemeinschaft (grants MO2192/8-1 to A.M. and SFB 840, project B8 to A.G.). We appreciate the support of the Keylab for optical and electron microscopy at the Bavarian Polymer Institute.

Open access funding enabled and organized by Projekt DEAL.

Conflict of Interest

The authors declare no conflict of interest.

Author Contributions

J.D. and C.L. contributed equally to this work. J. D. and C. L. contributed equally to the results of the manuscript. J.D. and S.F. cloned, expressed, purified, and analyzed LOV proteins; C.L. synthesized, derivatized, and analyzed AuNP. J.D., C.L., and S.F. assessed the light-dependent interplay of protein and nanoparticles and evaluated data. A-K.M., J.D., and C.L. performed and analyzed the AF4 measurements. J.D. and C.L. prepared figures. A.M. and A.G. conceived and supervised the project. J.D., C.L., A.M., and A.G. wrote the manuscript with input from all authors.

Data Availability Statement

All data underlying the main text and the supplementary materials are available as a supplementary zip archive.

Keywords

assembly, gold nanoparticles, photoresponsive materials, sensory photoreceptors, smart materials

Received: July 7, 2020
Revised: October 22, 2020
Published online:

[1] J. M. Christie, P. Reymond, G. K. Powell, P. Bernasconi, A. A. Raibekas, E. Liscum, W. R. Briggs, *Science* **1998**, *282*, 1698.
[2] A. Losi, K. H. Gardner, A. Möglich, *Chem. Rev.* **2018**, *118*, 10659.
[3] G. Chen, I. Roy, C. Yang, P. N. Prasad, *Chem. Rev.* **2016**, *116*, 2826.
[4] W. J. Stark, P. R. Stoessel, W. Wohlleben, A. Hafner, *Chem. Soc. Rev.* **2015**, *44*, 5793.
[5] N. L. Rosi, C. A. Mirkin, *Chem. Rev.* **2005**, *105*, 1547.
[6] C. J. Murphy, A. M. Gole, J. W. Stone, P. N. Sisco, A. M. Alkilany, E. C. Goldsmith, S. C. Baxter, *Acc. Chem. Res.* **2008**, *41*, 1721.
[7] C.-A. J. Lin, T.-Y. Yang, C.-H. Lee, S. H. Huang, R. A. Sperling, M. Zanella, J. K. Li, J.-L. Shen, H.-H. Wang, H.-I. Yeh, W. J. Parak, W. H. Chang, *ACS Nano* **2009**, *3*, 395.
[8] G. Han, P. Ghosh, V. M. Rotello, *Future Med.* **2007**, *2*, 113.
[9] N. L. Rosi, D. A. Giljohann, C. S. Thaxton, A. K. R. Lytton-Jean, M. S. Han, C. A. Mirkin, *Science* **2006**, *312*, 1027.
[10] C. Xu, K. Xu, H. Gu, X. Zhong, Z. Guo, R. Zheng, X. Zhang, B. Xu, *J. Am. Chem. Soc.* **2004**, *126*, 3392.
[11] Z. Fan, X. Chen, M. Köhn Serrano, H. Schmalz, S. Rosenfeldt, S. Förster, S. Agarwal, A. Greiner, *Angew. Chem., Int. Ed.* **2015**, *54*, 14539.
[12] Z. Fan, M. K. Serrano, A. Schaper, S. Agarwal, A. Greiner, *Adv. Mater.* **2015**, *27*, 3888.
[13] Y. Ofir, B. Samanta, V. M. Rotello, *Chem. Soc. Rev.* **2008**, *37*, 1814.
[14] Q.-Y. Lin, J. A. Mason, Z. Li, W. Zhou, M. N. O'Brien, K. A. Brown, M. R. Jones, S. Butun, B. Lee, V. P. Dravid, K. Aydin, C. A. Mirkin, *Science* **2018**, *359*, 669.

[15] M. S. Köhn Serrano, T. A. F. König, J. S. Haataja, T. I. Löbling, H. Schmalz, S. Agarwal, A. Fery, A. Greiner, *Macromol. Rapid Commun.* **2016**, *37*, 215.
[16] L. Zhang, L. Dai, Y. Rong, Z. Liu, D. Tong, Y. Huang, T. Chen, *Langmuir* **2015**, *31*, 1164.
[17] P. K. Kundu, D. Samanta, R. Leizrowice, B. Margulis, H. Zhao, M. Börner, T. Udayabhaskararao, D. Manna, R. Klajn, *Nat. Chem.* **2015**, *7*, 646.
[18] Y. Chen, Z. Wang, Y. He, Y. J. Yoon, J. Jung, G. Zhang, Z. Lin, *Proc. Natl. Acad. Sci.* **2018**, *115*, 1391.
[19] J.-Y. Kim, J. Yeom, G. Zhao, H. Calcaterra, J. Munn, P. Zhang, N. Kotov, *J. Am. Chem. Soc.* **2019**, *141*, 11739.
[20] Q. Wang, D. Li, J. Xiao, F. Guo, L. Qi, *Nano Res.* **2019**, *12*, 1563.
[21] J. M. Abad, S. F. L. Mertens, M. Pita, V. M. Fernández, D. J. Schiffrin, *J. Am. Chem. Soc.* **2005**, *127*, 5689.
[22] D. Huebner, C. Rossner, P. Vana, *Polymer* **2016**, *107*, 503.
[23] J. Lai, Y. Xu, X. Mu, X. Wu, C. Li, J. Zheng, C. Wu, J. Chen, Y. Zhao, *Chem. Commun.* **2011**, *47*, 3822.
[24] E. Jaquay, L. J. Martínez, N. Huang, C. A. Mejia, D. Sarkar, M. L. Povinelli, *Nano Lett.* **2014**, *14*, 5184.
[25] S. Christau, T. Moeller, J. Genzer, R. Koehler, R. vonKlitzing, *Macromolecules* **2017**, *50*, 7333.
[26] R. Pamies, J. G. H. Cifre, V. F. Espín, M. Collado-González, F. G. D. Baños, J. G. de laTorre, *J. Nanoparticle Res.* **2014**, *16*, 2376.
[27] H.-Y. Park, K. Kim, S. Hong, H. Kim, Y. Choi, J. Ryu, D. Kwon, R. Grailhe, R. Song, *Langmuir* **2010**, *26*, 7327.
[28] E. Herman, M. Sachse, P. G. Kroth, T. Kottke, *Biochemistry* **2013**, *52*, 3094.
[29] B. D. Zoltowski, B. R. Crane, *Biochemistry* **2008**, *47*, 7012.
[30] A. Banerjee, E. Herman, T. Kottke, L.-O. Essen, *Structure* **2016**, *24*, 171.
[31] U. Heintz, I. Schlichting, *eLife* **2016**, *5*, 11860.
[32] X. Wang, X. Chen, Y. Yang, *Nat. Methods* **2012**, *9*, 266.
[33] G. Frens, *Nat. Phys. Sci.* **1973**, *241*, 20.
[34] S. Panigrahi, S. Basu, S. Praharaj, S. Pande, S. Jana, A. Pal, S. K. Ghosh, T. Pal, *J. Phys. Chem. C* **2007**, *111*, 4596.
[35] P. Kalimuthu, S. A. John, *Mater. Chem. Phys.* **2010**, *122*, 380.
[36] A. M. Smith, L. E. Marbella, K. A. Johnston, M. J. Hartmann, S. E. Crawford, L. M. Kozycz, D. S. Seferos, J. E. Millstone, *Anal. Chem.* **2015**, *87*, 2771.
[37] F. Chen, S. V. Wegner, *ACS Synth. Biol.* **2020**, *9*, 1169.
[38] T. Ziegler, A. Möglich, *Front. Mol. Biosci.* **2015**, *2*, 30.
[39] A. Pudasaini, K. K. El-Arab, B. D. Zoltowski, *Front. Mol. Biosci.* **2015**, *2*, 18.
[40] D. G. Gibson, L. Young, R.-Y. Chuang, J. C. Venter, C. A. Hutchison, H. O. Smith, *Nat. Methods* **2009**, *6*, 343.
[41] T. Mathes, C. Vogl, J. Stolz, P. Hegemann, *J. Mol. Biol.* **2009**, *385*, 1511.
[42] X. Liu, M. Atwater, J. Wang, Q. Huo, *Colloids Surf., B* **2007**, *58*, 3.